

Preparation and phase transformation of highly ordered TiO₂ nanodot arrays on sapphire substrates

Po-Lin Chen, Cheng-Tzu Kuo, Fu-Ming Pan, and Tzeng-Guang Tsai

Citation: *Applied Physics Letters* **84**, 3888 (2004); doi: 10.1063/1.1738941

View online: <http://dx.doi.org/10.1063/1.1738941>

View Table of Contents: <http://scitation.aip.org/content/aip/journal/apl/84/19?ver=pdfcov>

Published by the [AIP Publishing](#)

Articles you may be interested in

[A review of TiO₂ nanotube arrays for hydrogen sensing application](#)

AIP Conf. Proc. **1482**, 611 (2012); 10.1063/1.4757544

[Theoretical investigation of size and shape effects on the melting temperature and energy bandgap of TiO₂ nanostructures](#)

Appl. Phys. Lett. **92**, 103121 (2008); 10.1063/1.2897297

[Effect of anodic TiO₂ powder as additive on electron transport properties in nanocrystalline TiO₂ dye-sensitized solar cells](#)

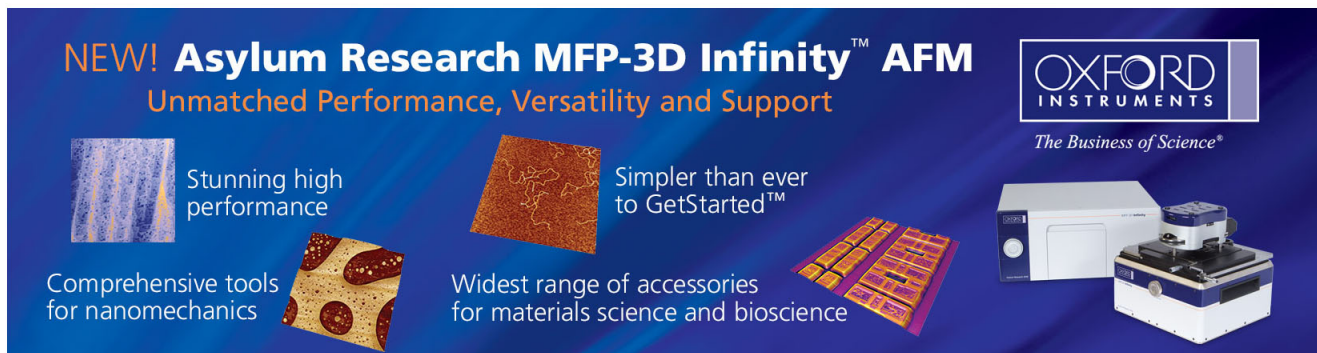
Appl. Phys. Lett. **91**, 233120 (2007); 10.1063/1.2823604

[High efficiency double heterojunction polymer photovoltaic cells using highly ordered TiO₂ nanotube arrays](#)

Appl. Phys. Lett. **91**, 152111 (2007); 10.1063/1.2799257

[Preparation of thermally stable TiO₂-terminated SrTiO₃ \(100\) substrate surfaces](#)

Appl. Phys. Lett. **85**, 272 (2004); 10.1063/1.1771461

The advertisement features a dark blue background with white and orange text. At the top left, it reads 'NEW! Asylum Research MFP-3D Infinity™ AFM' in large white letters, followed by 'Unmatched Performance, Versatility and Support' in orange. On the right, the 'OXFORD INSTRUMENTS' logo is shown in white, with the tagline 'The Business of Science®' below it. The central part of the ad is divided into four quadrants, each with an image and text: top-left shows a textured surface with the text 'Stunning high performance'; top-right shows a brown, porous-looking surface with 'Simpler than ever to GetStarted™'; bottom-left shows a pattern of red and white circles with 'Comprehensive tools for nanomechanics'; bottom-right shows a grid of small, colorful rectangular samples with 'Widest range of accessories for materials science and bioscience'. On the far right, there is a photograph of the MFP-3D Infinity AFM instrument, a white and blue device with a sample stage.

Preparation and phase transformation of highly ordered TiO₂ nanodot arrays on sapphire substrates

Po-Lin Chen, Cheng-Tzu Kuo,^{a)} and Fu-Ming Pan

Department of Materials Science and Engineering, National Chiao Tung University, Hsinchu, Taiwan

Tzeng-Guang Tsai

AU Optronics Corp., Science-Based Industrial Park, Hsinchu, Taiwan

(Received 7 January 2004; accepted 11 March 2004; published online 29 April 2004)

Ordered nanodot arrays of titanium oxide (TiO₂) were prepared from an epitaxial Al/TiN bilayered film on a sapphire substrate by electrochemical anodization of the TiN layer using a nanoporous anodic aluminum oxide (AAO) film as the template. The nanodots with an average diameter of about 60 nm can faithfully duplicate the size, shape, and hexagonal pore pattern of the AAO nanopores. The phase development of the isolated TiO₂ nanodots is very much different from TiO₂ thin films and powders. After high temperature annealing, the nanodots are polycrystalline and consist of a mixed phase of anatase and rutile instead of single rutile phase. We expect that TiO₂ nanodots with a single phase of anatase can be realized as long as the size of the nanodots is smaller than the critical nuclei size for rutile formation. © 2004 American Institute of Physics.

[DOI: 10.1063/1.1738941]

Titanium oxide (TiO₂) is one of the most important transition metal oxides, which has been proposed for a wide range of uses including photocatalysts,^{1,2} photoelectrochemical cells,³ gas detectors,⁴ antireflection coatings,⁵ and high- κ dielectrics.⁶ In recent years, nanometer-sized tubules,⁷ wires,⁸ and particles^{9,10} of TiO₂ have been intensively studied because of the large surface area and quantum size effects, which result in chemical, optical, and electrical properties. The majority of previous studies used sol-gel⁷ or hydrolysis process^{8,11} to prepare TiO₂ nanostructures. In order to well control the dimension and morphology of TiO₂ nanostructures, nanoporous anodic aluminum oxide (AAO) has been widely utilized as a template to selectively grow TiO₂ within the nanopores. In our previous study, we employed nanoporous AAO films as the mask for local anodic oxidation of titanium nitride (TiN) films to fabricate ordered nanodot arrays of TiO₂.¹² Self-organized nanodot arrays of TiO₂ are formed by electrochemical anodization of an Al/TiN bilayered film on the silicon substrate. When anodization of the Al upper layer is complete, anodic oxidation of the underlying TiN layer is confined in the pore area of the initially formed AAO, resulting in TiO₂ nanodot arrays with a uniform size distribution in accordance with the hexagonal order and pore size of the AAO nanopores. However, the nanodots are irregular in shape because the rough interface between the Al and TiN layers of the Al/TiN film stack results in a nonuniform anodic oxidation rate in the TiN layer. In this letter, we report on the realization of highly ordered TiO₂ nanodots with uniform shape on a sapphire substrate by anodization of an epitaxial Al/TiN film stack. Since the as-prepared TiO₂ nanodots are basically amorphous, the post-growth annealing effect on phase development of the nanodots is discussed.

Fabrication of the TiO₂ nanodot arrays began with the

epitaxial growth of a 10-nm-thick TiN film on (0001)-oriented sapphire wafers using a reactive dc magnetron sputtering system. Following the TiN deposition, an Al film ~5 μ m in thickness was deposited by thermal evaporation in a high vacuum chamber ($<5 \times 10^{-7}$ Torr). The crystallinity and orientation of the as-deposited films were investigated by x-ray diffraction (XRD) (Philips X'Pert Pro). Figure 1 shows the XRD θ - 2θ scan spectrum of the Al/TiN/sapphire heterostructure. In addition to the sapphire (0006) peak, only TiN (111) and Al (111) peaks are present in the XRD spectrum. The preferential growth of the (111) TiN and (111) Al films suggests epitaxial growth in sequence of the film stack on the (0001) sapphire. Although the lattice mismatch between the (111) plane of the TiN film and the (0001) plane of sapphire is as high as 8.46%, misfit dislocations arranged almost periodically on the interface can relieve the lattice mismatch.¹³

For preparation of TiO₂ nanodot arrays, the as-deposited Al/TiN bilayered films were directly oxidized by electrochemical anodization without any preplanarization step. An-

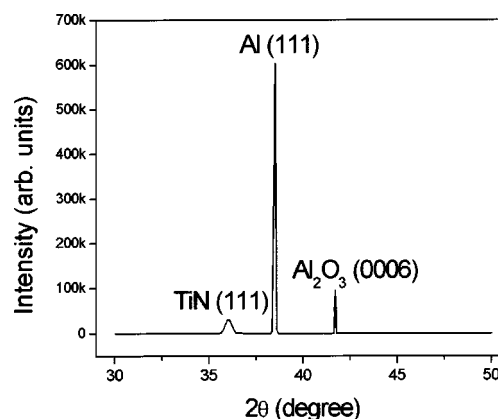


FIG. 1. XRD θ - 2θ scan of an epitaxial Al/TiN bilayer grown on sapphire (0001).

^{a)}Electronic mail: ctkuo@mail.nctu.edu.tw

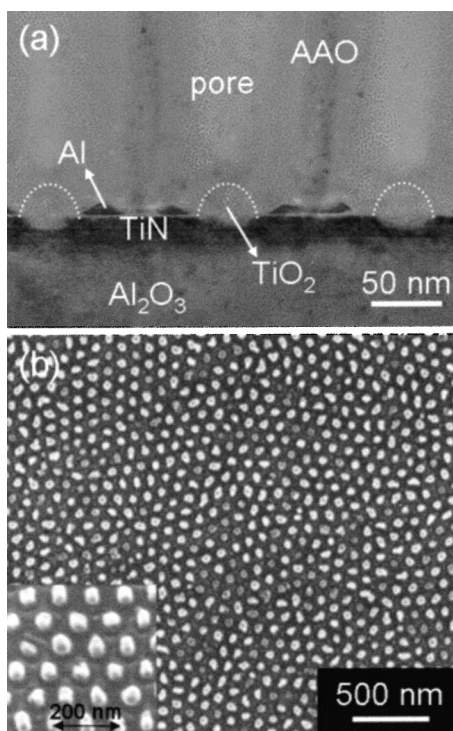


FIG. 2. (a) Cross-sectional TEM image of the bottom of AAO nanopore channels after the completion of the anodization. The dashed lines indicate the interface between TiO_2 nanodot and Al_2O_3 barrier layer; (b) top-view FE-SEM image of the TiO_2 nanodot arrays after the nanoporous AAO template was removed by a mixed solution of H_3PO_4 and CrO_3 . The inset is the side-view image of the nanodots.

odization was carried out in a 0.3 M oxalic acid solution at 21 °C under a constant polarization voltage of 40 V. The anodization process can be divided into two oxidation stages, i.e., anodic oxidations of the Al layer and the underlying TiN layer. In the first stage, the upper Al layer was anodized to nanoporous AAO containing a scalloped hemispherical oxide barrier under each pore bottom. As the downward grown pore channels reached the Al/TiN interface, the underlying TiN layer was oxidized by anodization as well. The anodic reaction was terminated while the exposed TiN region was fully oxidized to TiO_2 . Figure 2(a) shows a cross-sectional transmission electron microscopy (TEM) (JEOL JEM-2010F) image of the bottom of AAO nanopores after the anodization. The anodic oxidation of the TiN layer was confined in the AAO pore area and thereby isolated TiO_2 dome structures were formed at the interface between the AAO and TiN layers. At the end of the anodization, the TiO_2 dome is surrounded by unanodized Al and mantled by Al_2O_3 barrier. Chemical phases labeled in Fig. 2(a) were characterized by electron energy loss spectroscopy (EELS) and energy dispersive spectroscopy (EDS).

Figure 2(b) shows the top-view field-emission scanning electron microscopy (FE-SEM) image of the TiO_2 nanodot arrays after removing the nanoporous AAO. The self-organized nanodots have a uniform size distribution with a diameter of about 60 nm and an interdot distance of about 100 nm. The nanodots are grouped into domains, and within a dot array domain, ordered nanodots with a hexagonal arrangement can be clearly observed. Most nanodots duplicate the circular shape of the AAO nanopores except those at domain boundaries. The morphology of the TiO_2 nanodots

should be strongly affected by the diffusion path of oxygen-containing ions (O^{2-} and/or OH^- from electrolyte) near the Al/TiN interface of the Al/TiN film stack because the oxidation rate of the TiN layer is mainly determined by the concentration of $\text{O}^{2-}/\text{OH}^-$ ions nearby.¹⁴ A rough interface between the Al and TiN layers leads to a nonuniform diffusion rate of $\text{O}^{2-}/\text{OH}^-$ ions at the interface and thus results in irregular ion concentration distribution around the growing nanodots. In the previous study, nanodots prepared from a polycrystalline Al/TiN film stack had an irregular dome shape with a coarse base structure,¹² which is primarily a reflection of the rough interface between the Al and TiN layers. In addition, the polycrystalline Al/TiN interface has a higher defect density (such as grain boundary, dislocation, vacancy, etc.) leading to a nonuniform ion transport through the interface. In grain boundaries, the diffusion coefficient of oxygen species is several orders of magnitude greater than that of volume diffusion coefficient.¹⁵ Migration of $\text{O}^{2-}/\text{OH}^-$ ions is more rapid along grain boundaries, dislocations, and external surfaces than in the interior of crystals, resulting in the formation of TiO_2 nanodots with a rough dome structure could not faithfully duplicate the circular shape of the AAO nanopores. In contrast, the epitaxial Al/TiN film stack has a smoother interface and lower defect density, and, therefore, can produce circular nanodots with a smoother surface.

TiO_2 has three crystalline phases, i.e., rutile, anatase, and brookite. Rutile is the thermodynamically stable phase in all temperatures and pressures, while anatase and brookite are metastable phases.¹⁶ Anatase is the TiO_2 phase of the greatest commercial interest, although it is seldom found in natural ore. The as-prepared TiO_2 nanodots in this study are basically amorphous, but they can later be converted to crystalline TiO_2 by annealing. Prior to annealing, unanodized Al and TiN surrounding the TiO_2 nanodots were removed by reactive ion etch (RIE) using a gas mixture of Cl_2 and BCl_3 . Annealing was performed at temperature higher than 900 °C in a furnace with a flowing oxygen atmosphere for 1 h. The XRD θ - 2θ scan spectra of the TiO_2 nanodot arrays after annealing are shown in Fig. 3(a). After annealing at 900 °C, obvious diffraction peaks of anatase (112) and rutile (210) are observed, indicating that polycrystalline TiO_2 nanodots are formed. Figure 3(b) shows the high-resolution TEM (HRTEM) image of the TiO_2 nanodot/sapphire interface. Two enlarged images defined by the dashed rectangles in Fig. 3(b) are given in Figs. 3(c) and 3(d). The lattice fringes with a spacing of 4.76 Å in Fig. 3(c) and 3.24 Å in Fig. 3(d) corresponds to the spacing between the (002) planes of anatase and the (110) planes of rutile, respectively. From the HRTEM image, the polycrystalline nanodot consists of two dominant grains of anatase and rutile (grain boundary is marked by white arrows) accompanied by several smaller grains. When the nanodots are annealed at a higher temperature of 1200 °C, the XRD spectrum in Fig. 3(a) clearly shows that the anatase phase still exists and predominates over the rutile phase in the nanodots. Moreover, rutile gradually transferred the orientation from (210) to (200), which may result from a better lattice match between the rutile (200) and sapphire (0001) planes.¹⁷

The anatase-to-rutile phase transformation of TiO_2 is be-

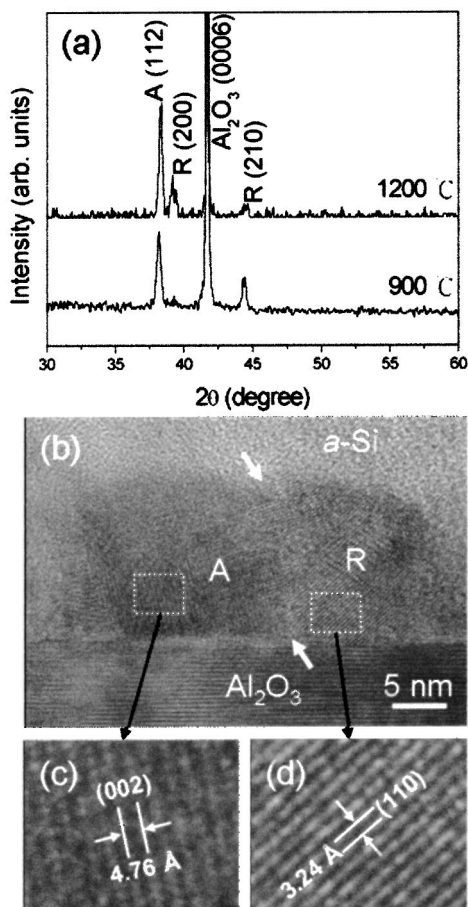


FIG. 3. (a) XRD θ - 2θ scan of the TiO₂ nanodot arrays after annealing in oxygen atmosphere for 1 h. The diffraction peaks for anatase phase and rutile phase are marked with A and R, respectively; (b) cross-sectional HRTEM image of the TiO₂ nanodot/sapphire interface. The sample was covered with an *a*-Si film to protect the nanodots. The grain boundary is indicated by two white arrows. Zoom-in images of the anatase grain and the rutile grain are presented in (c) and (d), respectively.

lied to be spontaneous, and is kinetically favorable at high temperatures.¹⁶ However, it is interesting to note that the TiO₂ nanodots formed in the study can maintain a stable anatase phase at temperatures as high as 1200 °C. This is quite different from the cases of TiO₂ thin films and powders. During the crystallization process of TiO₂ nanodots, anatase grains first nucleate and then grow to a critical size, which will in turn provide nucleation sites for the development of the rutile phase.¹⁸ When the anatase grain reaches a critical size, the transformation of anatase to rutile begins and proceeds very rapidly.¹⁹ The driving force for the phase transformation is the difference in free energies between the anatase and rutile phases. The rutile grain will keep growing at the expense of the surrounding anatase phase until the remaining anatase phase diminishes to a critical size. Zhang and Banfield, using thermodynamic analyses, proposed that the stability of the anatase phase depends largely on the grain (particle) size.²⁰ They suggested that when the particle size decreases below ~ 14 nm, the total free energy of rutile is higher than that of anatase. This is a consequence of the fact that rutile has a higher surface energy than anatase, and thus the relative phase stability of anatase and rutile reverses as

the particle size is reduced to a critical value. Since the TiO₂ nanodot is isolated, an increase in the volume of the rutile phase will lead to a decrease in the anatase content. As the size of the anatase grains is diminished to the critical size, the phase transformation is terminated, resulting in a stable coexistence of the two phases in the nanodots. Therefore, the anatase phase can exist in the TiO₂ nanodots even at a considerably high temperature. From the above discussion, we expect that the TiO₂ nanodots with a pure anatase phase may be accomplished when the size of the nanodots is smaller than the critical size for the rutile formation.

In summary, we have fabricated highly ordered nanodot arrays of TiO₂ prepared from an epitaxial Al/TiN film stack on a sapphire substrate by electrochemical anodization. The average size of the nanodots is about 60 nm with a hexagonal dot array pattern conformed to the upper nanoporous AAO layer. The epitaxial Al/TiN interface with a lower interfacial roughness and defect density provides a uniform diffusion rate of O²⁻/OH⁻ ions and, consequently, contributes to the formation of smooth nanodots. The XRD and HRTEM results confirm that the TiO₂ nanodots are polycrystalline in nature and mainly consist of two dominant grains of anatase and rutile phases after high temperature annealing. Because the high temperature crystallization process is confined in the isolated dome structure, the grain growth and a complete anatase-to-rutile phase transition are retarded, resulting in the coexistence of the anatase and rutile phases in the nanodots.

This work was supported partly by the National Science Council (NSC), Taiwan, under Contract Nos. NSC92-2216-E-009-010, NSC92-2216-E-009-009, and NSC92-2210-M-009-001.

- ¹A. Linsebigler, G. Lu, and J. T. Yates, *Chem. Rev.* (Washington, D.C.) **95**, 735 (1995).
- ²M. Anpo, T. Shima, S. Kodama, and Y. Kubokawa, *J. Phys. Chem.* **91**, 4305 (1987).
- ³M. Grätzel, *Nature* (London) **414**, 338 (2001).
- ⁴D. Manno, G. Micocci, R. Rella, A. Serra, A. Taurino, and A. Tepore, *J. Appl. Phys.* **82**, 54 (1997).
- ⁵G. Crotty, T. Daud, and R. Kachare, *J. Appl. Phys.* **61**, 3077 (1987).
- ⁶B. H. Lee, Y. Jeon, K. Zawadzki, W. J. Qi, and J. Lee, *Appl. Phys. Lett.* **74**, 3143 (1999).
- ⁷G. H. Du, Q. Chen, R. C. Che, Z. Y. Yuan, and L.-M. Peng, *Appl. Phys. Lett.* **79**, 3702 (2001).
- ⁸Y. Lei, L. D. Zhang, G. W. Meng, G. H. Li, X. Y. Zhang, C. H. Liang, W. Chen, and S. X. Wang, *Appl. Phys. Lett.* **78**, 1125 (2001).
- ⁹Z.-L. Hua, J.-L. Shi, L.-X. Zhang, M.-L. Ruan, and J.-N. Yan, *Adv. Mater.* (Weinheim, Ger.) **14**, 830 (2002).
- ¹⁰H. A. Bullen and S. J. Garrett, *Nano Lett.* **2**, 739 (2002).
- ¹¹X. Y. Zhang, L. D. Zhang, W. Chen, G. W. Meng, M. J. Zheng, and L. X. Zhao, *Chem. Mater.* **13**, 2511 (2001).
- ¹²P.-L. Chen, C.-T. Kuo, T.-G. Tsai, B.-W. Wu, C.-C. Hsu, and F.-M. Pan, *Appl. Phys. Lett.* **82**, 2796 (2003).
- ¹³W.-C. Chen, Y.-R. Lin, X.-J. Guo, and S.-T. Wu, *Jpn. J. Appl. Phys., Part 1* **42**, 208 (2003).
- ¹⁴O. Jessensky, F. Müller, and U. Gösele, *Appl. Phys. Lett.* **72**, 1173 (1998).
- ¹⁵J. R. Farver and R. A. Yund, *Earth Planet. Sci. Lett.* **161**, 189 (1998).
- ¹⁶K.-N. P. Kumar, *Scr. Metall. Mater.* **32**, 873 (1995).
- ¹⁷M. Schuisky, A. Härsta, A. Aidla, K. Kukli, A.-A. Kiisler, and J. Aarik, *J. Electrochem. Soc.* **147**, 3319 (2000).
- ¹⁸P. I. Gouma, P. K. Dutta, and M. J. Mills, *Nanostruct. Mater.* **11**, 1231 (1999).
- ¹⁹C.-C. Wang and J. Y. Ying, *Chem. Mater.* **11**, 3113 (1999).
- ²⁰H. Zhang and J. F. Banfield, *J. Mater. Chem.* **8**, 2073 (1998).